A System for Counting Fetal and Maternal Red Blood Cells

Ji Ge, *Member, IEEE*, Zheng Gong, *Member, IEEE*, Jun Chen, Jun Liu, *Student Member, IEEE*, John Nguyen, Zongyi Yang, Chen Wang, and Yu Sun*, *Senior Member, IEEE*

***Abstract*—The Kleihauer–Betke (KB) test is the standard method for quantitating fetal-maternal hemorrhage in maternal care. In hospitals, the KB test is performed by a certified technologist to count a minimum of 2000 fetal and maternal red blood cells (RBCs) on a blood smear. Manual counting suffers from inherent inconsistency and unreliability. This paper describes a system for automated counting and distinguishing fetal and maternal RBCs on clinical KB slides. A custom-adapted hardware platform is used for KB slide scanning and image capturing. Spatial-color pixel classification with spectral clustering is proposed to separate overlapping cells. Optimal clustering number and total cell number are obtained through maximizing cluster validity index. To accurately identify fetal RBCs from maternal RBCs, multiple features including cell size, roundness, gradient, and saturation difference between cell and whole slide are used in supervised learning to generate feature vectors, to tackle cell color, shape, and contrast variations across clinical KB slides. The results show that the automated system is capable of completing the counting of over 60 000 cells (versus ∼2000 by technologists) within 5 min (versus ∼15 min by technologists). The throughput is improved by approximately 90 times compared to manual reading by technologists. The counting results are highly accurate and correlate strongly with those from benchmarking flow cytometry measurement.**

***Index Terms*—Automation, fetal-maternal hemorrhage (FMH) quantification, fetal red blood cells, image processing, Kleihauer–Betke (KB) test, maternal red blood cells.**

I. Introduction

In North America, there are over 6 million pregnancies annually. Approximately 10% of all pregnancies in Caucasian populations are of an Rhesus D (RhD) negative woman with an RhD positive baby. These pregnancies are at risk of RhD hemolytic disease of the newborn. During pregnancy or child birth, small amounts of fetal blood can enter the maternal circulation (an event called fetal-maternal hemorrhage or FMH). The presence of fetal RhD-positive cells in her circulation can cause a mother who is RhD negative to mount an immune response, generating small amounts of antibodies (including IgG) against the RhD antigen. The generated antibodies destruct the RhD positive fetal red blood cells (RBCs) by passing through the placenta into the fetal bloodstream and lead to hemolysis [1]. FMH can have devastating consequences for RhD positive fetus, such as anemia, neurologic injury, stillbirth, and neonatal death. Hence, quantification of FMH is necessary for physicians to make treatment decisions, for instance, the administration of an appropriate therapeutic dose of RhD immune globulin to suppress sensitization of the maternal immune system [2]–[4].

Besides Rh diseases, FMH can also result from the loss of integrity of the normal physiological barrier between the fetal and maternal circulation, which must be quantified in pregnancy care for prompt treatment (e.g., blood transfusion) [5]. The standard clinical method of quantitating FMH is the Kleihauer–Betke (KB) test [6]. The test takes advantage of the differential resistance of fetal and adult hemoglobin (i.e., HbF and HbA) to acid (HbF is significantly more resistant). A standard blood smear is prepared from the mother's blood (1:1 dilution with PBS). After drying, staining, and incubating, the blood smear slides are counted under a microscope by certified personnel. Since the fetal hemoglobin is resistant to the citrate buffer, the resulting bright-pink cells are classified as fetal cells [see Fig. 1(a)]. The percentage of FMH can then be calculated [7].

In present clinical practice, fetal RBCs and total number of RBCs are manually estimated by certified technologists who look into the eyepieces of a microscope and count a minimum of 2000 cells. Inherently, manual KB test is subjective and inconsistent, which can often result in underestimation/overestimation of fetal RBC count and wide variations across technologists and hospitals [8].

Flow cytometry is an accepted benchmark technique for counting fetal and maternal RBCs, based on the fetal hemoglobin-specific antibody. The flow cytometric analysis of FMH involves multiple pretreatment steps, which requires more than 30-min preprocess and has high personnel skill requirements [9]. Due to these limitations, flow cytometry testing is typically unavailable during after hours in hospitals. The infrastructure cost along with operating and reagent costs also limits the clinical routine use of flow cytometry for KB tests [10]. The adoption of flow cytometry for fetal/maternal RBC

Manuscript received April 5, 2014; revised May 8, 2014; accepted May 23, 2014. Date of publication May 29, 2014; date of current version November 18, 2014. This work was supported by the Natural Sciences and Engineering Research Council of Canada through an Idea to Innovation Grant, by the University of Toronto through a Connaught Innovation Award, by the Canada Research Chairs Program and in part by National Natural Science Foundation of China under Grant 61305019. *Asterisk indicates corresponding author.*

J. Ge is with the Advanced Micro and Nanosystems Laboratory, University of Toronto, Toronto, ON M5S 3G8 ,Canada, and also with the College of Electrical Engineering and Automation, Jiangxi University of Science and Technology, Ganzhou 341000, China (e-mail: jige@mie.utoronto.ca).

Z. Gong, J. Chen, J. Liu, J. Nguyen, and Z. Yang are with the Advanced Micro and Nanosystems Laboratory, University of Toronto, Toronto, ON M5S 3G8, Canada (e-mail: zgong@mie.utoronto.ca; junchen@mie.utoronto.ca; ljun@mie.utoronto.ca; jhn.nguyen@mail.utoronto.ca; yangzongyi@hotmail.com).

C. Wang is with the Department of Pathology and Laboratory Medicine, Mount Sinai Hospital, Toronto, ON M5G 1X5, Canada (e-mail: cwang@mtsinai.on.ca).

*Y. Sun is with the Advanced Micro and Nanosystems Laboratory, University of Toronto, Toronto, ON M5S 3G8, Canada (e-mail: sun@mie.utoronto.ca).

Color versions of one or more of the figures in this paper are available online at http://ieeexplore.ieee.org.

Digital Object Identifier 10.1109/TBME.2014.2327198

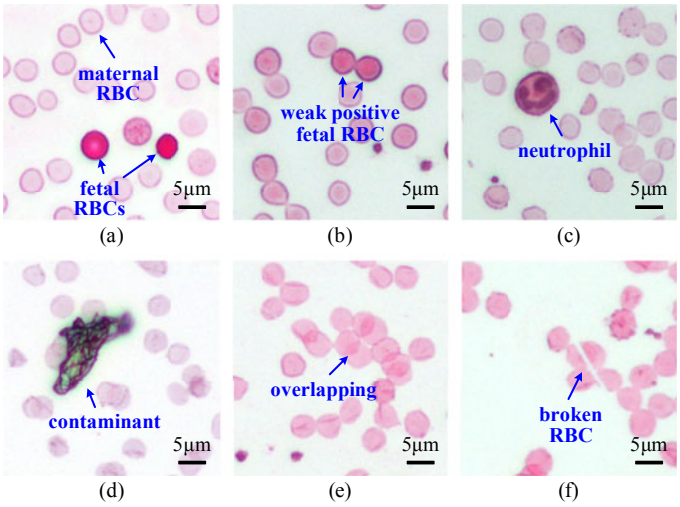

Fig. 1. Sample images from clinical KB slides. (a) "Canonical" fetal and maternal RBCs. (b) Weak positive fetal RBC. (c) Neutrophils. (d) Contaminant. (e) and (f) Severally overlapping and broken RBCs.

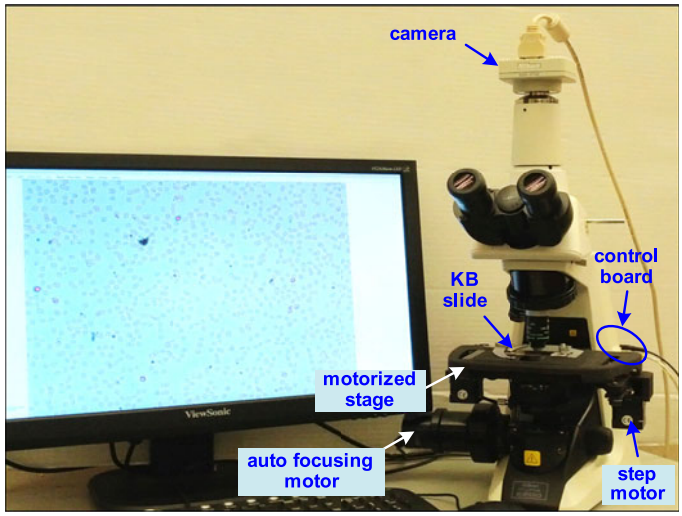

Fig. 2. System for automated image capturing and counting of fetal and maternal RBCs on clinical KB slides.

counting has been discussed for two decades in transfusion medicine [11]; however, the state-of-the-art practice in most hospitals for quantitating FMH is still manual KB test that relies on manual counting of fetal and maternal RBCs.

Fig. 1(a) shows canonical fetal and maternal RBCs that can be easily counted and distinguished. However, many KB slides have more complex patterns that make the tasks difficult. As shown in Fig. 1(b)–(f), KB slide preparation often results in cell overlapping; the presence of random contaminants; variations in cell color, size, and shape; contrast variations between cells and slide background across KB slides. Fetal RBC identification is also made challenging due to the existence of neutrophils and weak positive fetal RBCs. Automated RBC counting requires the segmentation of overlapping cells and the identification of fetal RBCs to be properly and reliably handled. A few attempts were made to automate fetal and maternal RBC counting [8], [12], where automation in these works refers to the use of commercial motorized stage to capture cell images. Fetal RBCs were distinguished from maternal RBCs based on intensity and distribution patterns of staining by a technologist. The total cell number on a KB slide was also manually estimated. No system exists that is capable of automated counting of total RBC numbers and fetal RBCs.

A number of image segmentation methods have been reported for cell counting. Nonmaximum suppression and seeded region growing were applied to segment corneal epithelial cells [6]. A critical issue in automated cell counting is effective segment overlapping cells. Major approaches for separating overlapping cells include watershed [13], template matching [14]–[16], and color-texture-based segmentation [17]. Due to the existence of regional maxima, the watershed algorithm often leads to oversegmentation. Template matching has low efficiency and requires large quantities of cell samples to achieve reasonable accuracy. Overlapping cells with close colors or textures can be clustered by color-texture-based segmentation [17]; however, they cannot be separated from each other for quantification.

Due to the complex characteristics of RBCs on clinical KB slides, spectral clustering (SC) with spatial-color information is proposed in this paper to segment overlapping cells. Each cell can be considered a cluster, since the color within a cell is relatively homogeneous. Besides color values, spatial information of each cell is also added to construct features used for generating similarity matrices. Cluster validity index is then used for determining the number of clusters.

To distinguish fetal RBCs from maternal RBCs, color information is the foremost cue. Due to variations in cell color, size, and the overlapping extent across KB slides, relying solely on saturation channel information is unreliable. Hence, the supervised clustering method is used in our system for fetal RBC identification, where feature vector is constructed with cell color, size, shape, gradient, and saturation difference between a cell and the whole slide.

II. System Design

As shown in Fig. 2, the system consists of a standard optical microscope, the manual stage of which was motorized with timing belts, pulleys, and stepping motors. The motorized stage has a positioning accuracy of ± 19 and ± 26 μm along the X- and Y-directions. The resolution is comparable for each direction and is 20 ± 3 μm. Travel distances for positioning a KB slide are 10 and 35 mm along X and Y, respectively.

Due to the nonuniform distribution of RBCs on a KB slide, which is more severe on the far left and far right parts of the slide, images should be captured around the slide center. Hence, two motion limit switches along the X- and Y-directions are added for automatic slide centering. A Z-motor is also added to the microscope for keeping images in focus during KB slide scanning. Autofocusing is conducted with the normalized variance focus algorithm [18]. Under a $20\times$ objective, the

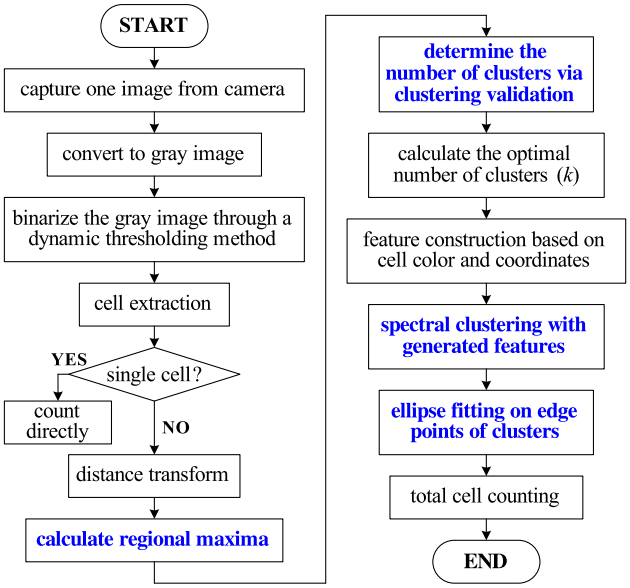

Fig. 3. Flowchart of total RBC counting.

system typically captures ∼120 images around the slide center (image size: 2560 × 1920) for automated counting.

III. Total RBC Counting

Fig. 1(e) shows an example of cell overlapping that must be reliably handled to achieve accurate counting of the total number of RBCs. To begin with, a target needs to be determined to be an isolated cell or overlap with other cells. For this purpose, we use the concavity points searching method [19]. If a cell is isolated without any concavity points, the cell is counted as one cell directly. Otherwise, segmentation as discussed below is conducted.

In overlapping RBCs, each cell forms a cluster due to the similar color within the same cell. Hence, segmenting overlapping cells can be considered cluster analysis. Among existing clustering methods, the k-means algorithm is effective only for clusters with similar sizes and densities, a condition that is not true in overlapping RBCs on a KB slide. Furthermore, the k-means algorithm is sensitive to initial centers and usually converges to a local optimum. In comparison, the SC algorithm [20] is capable of recognizing clusters with unusual shapes and obtaining global optimal solutions with eigendecomposition. Unfortunately, only depending on cell color, the SC algorithm can mistakenly group those pixels belonging to different RBCs, although they locate far from each other in the image.

Hence, in our system, spatial information (i.e., pixel coordinates) besides color is used to generate feature vectors used for calculating the similarity matrix of SC. This spatial and color-based SC approach is proven in our work effective in separating overlapping RBCs. Fig. 3 shows the sequence of processing for counting the total number of RBCs on a KB slide. Key steps are highlighted in blue and described in the following sections.

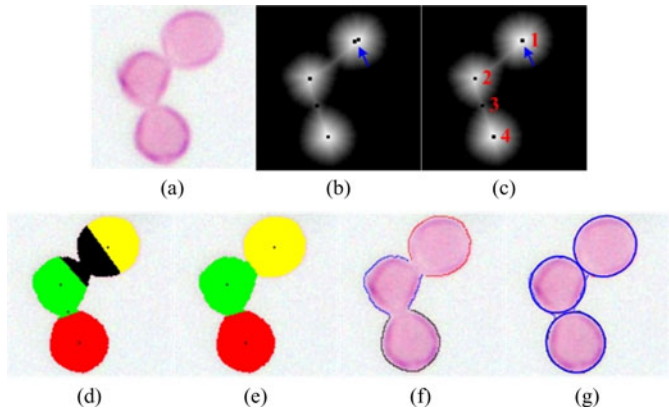

Fig. 4. Cluster number determination. (a) Original image. (b) Regional maxima (blue arrow labeled). (c) Spurious maxima eliminated. (d) SC result with $k = 4$. (e) SC result with $k = 3$, maximal SV value is 0.5198. (f) Edge points with three clusters (labeled in red, blue, and black). (g) After ellipse fitting.

A. Regional Maxima Preprocessing

We observed that many extracted regional maxima in a distance image are located closely [see Fig. 4(b)]. If overlapping cells are segmented directly with the number of regional maxima, oversegmentation often occurs. Thus, we defined a distance-dependent rule to eliminate those spurious maxima.

repeat
  $\forall m = (x_m, y_m) \in S$
 if $\exists n = \{(x_n, y_n) | D(m,n) \leqslant D_{TH})\}$ **then**
  select $p = \{m, n | max(x_m, x_n)\}$
  update S
 end if
until no changes in S

where m and n are regional maxima within maxima set S, D is the Euclidean distance between two arbitrary maxima, and D_{TH} is the minimal distance threshold. Considering that the radius of typical RBCs is approximately 20 pixels under a 20× microscope objective, D_{TH} in our system is set to 10. If the Euclidean distance $D(m, n)$ between point m and n is smaller than 10, the point with larger coordinate in the x-direction is selected into the set S (see Lines 3 and 4 of the rule). Fig. 4(c) shows that spurious maxima are removed after regional maxima preprocessing.

B. Determination of Optimal Number of Clusters

In cluster analysis of overlapping cells, the initial number of clusters is obtained through counting the number of local maxima after regional maxima preprocessing, and then, cluster validation is applied to determine the number of overlapping cells. Cluster validity index SV [21], consisting of two evaluation criteria of the cells (i.e., separation S and compactness V), is

$$SV(k, V, P) = \frac{S_k}{V_k} = \frac{\sum_{i=1}^{k} \min\limits_{j \in [1,\ldots,k], i \neq j} d(v_i, v_j)}{\sum_{i=1}^{k} \max\limits_{p_j \in C_i} d(p_j, v_i)} \quad (1)$$

TABLE I
DIFFERENT SV VALUES AND NUMBER OF CLUSTERS DETERMINED

SV ($k=4$)	SV ($k=3$)	SV ($k=2$)
0.3275 (1,2,3,4)	0.3581 (1,2,3)	0.2758 (1,2)
/	**0.5198 (1,2,4)**	0.3212 (1,3)
/	0.3862 (1,3,4)	0.3849 (1,4)
/	0.2723 (2,3,4)	0.1431 (2,3)
/	/	0.2770 (2,4)
/	/	0.1380 (3,3)

where $P = \{p_j;\ j = 1, 2, \ldots, n\}$ denotes the dataset with n data points. Dataset P can then be partitioned into k clusters C_i and each cluster has a centroid v_i, here $i = 1, 2, \ldots, k$. Separation measure S_k is the sum of pairwise minimal intercluster distances in a k-cluster structure, while compactness measure V_k indicates how different the members of each cluster are. The smaller the value of V_k, the compacter the clusters. The optimal cell number is obtained through maximizing the SV index.

Fig. 4 shows an example, where SV values of the overlapping RBCs are calculated and summarized in Table I. For each SV value, corresponding cluster centroids are given in parentheses in the table. As shown in Table I, the maximal SV value is 0.5198, with point 1, 2, and 4 (labeled in Fig. 4) determined as cluster centroids, representing proper segmentation. In Fig. 4(e), after determining the optimal number of clusters and generating features based on cell color and spatial coordinates, the system applies SC to classify the overlapping cells (labeled red, green, and yellow). Subsequently, contours in the overlapped areas are predicted via ellipse fitting [22] [see Fig. 4(g)], since most RBCs on a KB slide have circle-like or ellipse-like shapes.

IV. FETAL RBC IDENTIFICATION

In the manual KB test, fetal RBC identification is conducted through human visual inspection relying on cell patterns such as color, size, shape, and texture [8]. However, feature variations across KB slides exist, although hospital technologists closely follow slide preparation protocols. In our system, supervised learning is used, and the process is illustrated in Fig. 5.

As shown in Fig. 5, all the 120 raw color images are read into the memory and converted to the hue saturation value (HSV) color space. An ($N \times 3$)-dimensional matrix M_1 constructed with all image pixels' H, S, and V values is fit with a two-component Gaussian mixture distribution. Here, N is equal to $2560 \times 1920 \times 120$, and Model 1 is generated for separating all RBC pixels from background pixels. In the converted color space, fetal and maternal RBCs show significant differences in the saturation channel. Therefore, combining saturation values of the cells singled out by Model 1 forms $N_{S\text{cell}} \times 1$ matrix M_2. Model 2 is generated for separating fetal RBCs from maternal RBCs, fit with another two-component Gaussian mixture distribution.

In captured color images, fetal RBCs appear red-colored, brilliant, shining, and smooth inside, while maternal ones appear light and pinkish. Therefore, color information is used to identify fetal cells. Due to cell variations across KB slides, besides

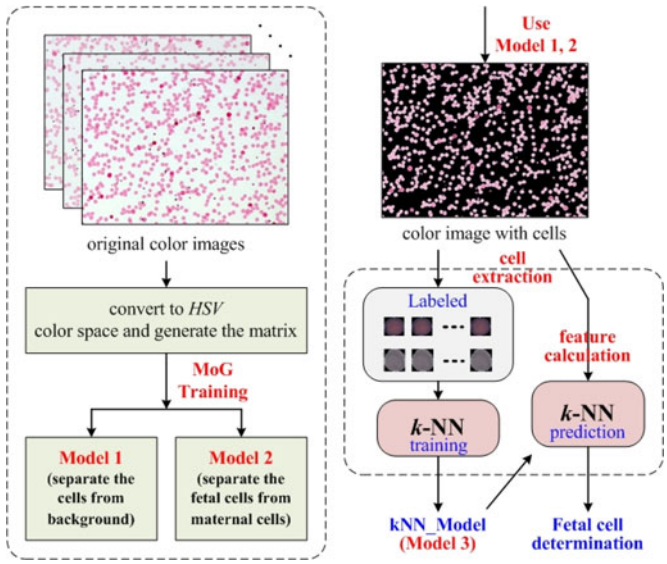

Fig. 5. Flowchart of supervised learning for distinguishing fetal RBCs and maternal RBCs.

color information, our system also integrates other features, such as cell size, roundness, gradient, and saturation difference between a cell and the whole slide, to distinguish fetal RBCs from maternal ones. Based on these features, the system applies a nonparametric learning algorithm [k-nearest neighbor (kNN)] via supervised learning to improve RBC classification accuracy. The kNN method is suitable for this purpose, since it is not certain whether the generated feature vectors of the fetal or maternal RBCs will satisfy such assumptions as Gaussian mixtures and linear separation. Additionally, the kNN method does not generalize the many training vectors and makes decisions based on the entire training feature vectors.

In this paper, more than 3500 cells (labeled "positive" or "negative") were calculated for generating feature vectors:

$$\begin{aligned}\text{Feature} &= (\text{HSV}_i, \text{RGB}_i, Gd_i, A_i, Rd_i, D_i) \\ &= \begin{pmatrix} hsv_1 & rgb_1 & gd_1 & a_1 & rd_1 & d_1 \\ \vdots & \vdots & \vdots & \vdots & \vdots & \vdots \\ hsv_i & rgb_i & gd_i & a_i & rd_i & d_i \end{pmatrix} \end{aligned} \quad (2)$$

where $i = 3500$; H, S, V, R, G, and B denote six channel values in HSV and RGB color space; Gd, A, and Rd are the gradient, area, and roundness of the cell, respectively; and D is the saturation difference between cell and whole slide.

A kNN model (Model 3) is built after fitting the feature vector with the kNN algorithm. Features of extracted cells are calculated and predicted with Model 3, where similarity of RBCs is calculated and verified according to

$$\begin{cases} \varsigma_{FC}^{i} = 1, & p_i > Th_f \\ \varsigma_{FC}^{i} = 0, & \text{others} \end{cases} \quad (3)$$

where $\varsigma_{\text{FC}}^{i}$ denotes the fetal RBC indicator of ith cell. p_i represents similarity between ith cell and labeled "positive" cells. Th_f denotes the fetal RBC threshold value. Typically, this threshold value is set to 0.5 according to statistical characteristics

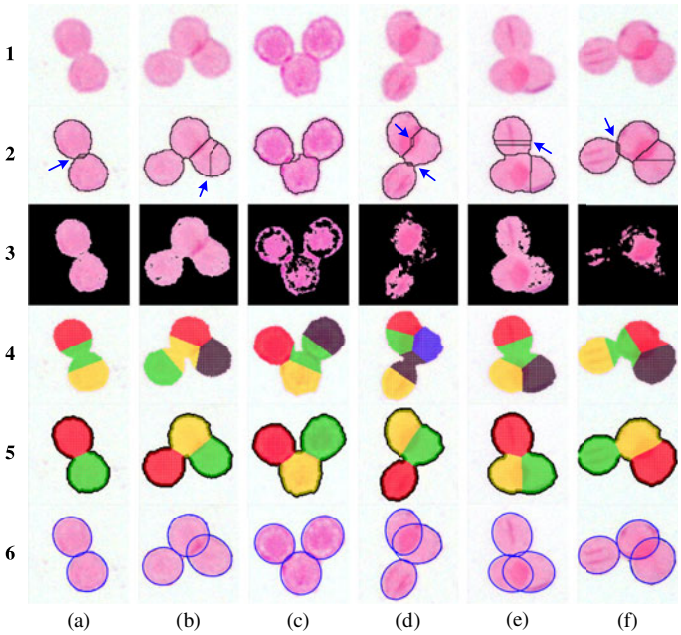

Fig. 6. Segmentation results using different algorithms. (1) Original image; (2) marker-controlled watershed [13]; (3) color- and texture-based segmentation [17]; (4) k-means algorithm; (5) and (6) our proposed spatial-color-based SC; and ellipse fitting on cell contours.

gathered from more than 50 clinical KB slides. Therefore, fetal RBC number is determined by $\sum_{i=1}^{N} \varsigma_{\mathrm{FC}}^{i}$, where N is the total cell number in the 120 images.

V. Experimental Results and Discussion

A. Total RBC Counting

Fig. 6 shows overlapping cells randomly selected from KB slides. Comparisons between marker-controlled watershed [13], color- and texture-based segmentation algorithm [17], k-means clustering algorithm, and our proposed spatial-color-based SC approach are made, as shown in Fig. 6.

Columns (a)–(c) in Fig. 6 show slightly overlapping situations where almost all the algorithms segmented cells reasonably well, except that oversegmentation occurred in (2, a) and (2, b) due to the wrong markers that existed within the overlapping area. For the more severally overlapping situations [see columns (d)–(f)], marker-controlled watershed in row 2 yielded oversegmentation due to many spurious maxima that appeared in the overlapping areas. k-means clustering in row 4 divided the overlapping cells into several regions; however, it led to erroneous segmentations due to the incorrect initial centers and number of clusters.

Most cell pixels were extracted with the color and texture clustering method, as shown in (3, a), (3, b), and (3, e). Unfortunately, only some scattered pixels or contours were picked out in other three columns in row 3, due to color and texture unevenness of the RBCs. This algorithm can extract the cells out but is not effective in separating them from each other. Our proposed algorithm (spatial-color-based SC) generates a new feature vector by adding spatial information into the original color matrix, which is proven effective in segmenting overlapping cells (see row 5 in Fig. 6). Furthermore, contour fitting on the overlapping cells generates clear ellipse-like contours for cell quantification.

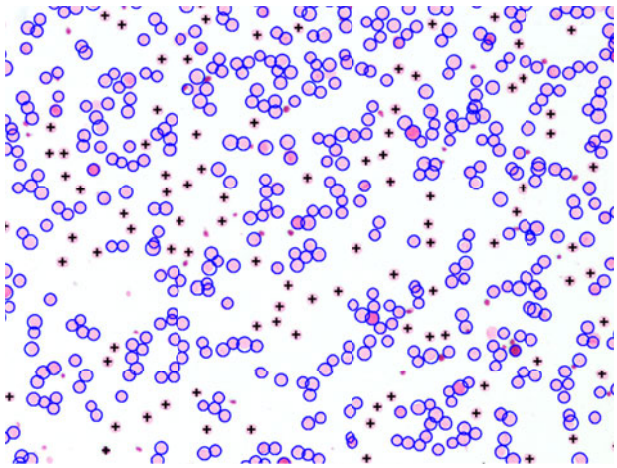

Fig. 7. Automated total RBC counting. The overlapping cells were segmented with proposed method, and their contours were labeled with blue ellipses. Those isolated RBCs, labeled with black plus symbols, were counted directly without segmentation procedures.

Fig. 7 shows the segmentation and counting results of one KB image. The overlapping cells were segmented, and their contours were labeled with blue ellipses. Those isolated cells, labeled with black plus symbols, were counted directly without segmentation procedures. To evaluate the accuracy of total RBC counting, 12 KB images were randomly selected and counted with the marker-controlled watershed method, our proposed spatial-color SC algorithm, and manual counting. Manual counting was conducted by a skilled technologist who used computer mouse clicking to count every cell in the images and then spent significant time carefully verifying every single cell. The manual counting results were used to calculate overcounting and undercounting rates summarized in Table II.

The marker-controlled watershed algorithm resulted in much higher overcounting ratios, ranging from 9.7% to 18.32%, due to its nature in severe oversegmentation. Our proposed algorithm performed significantly better in terms of both overcounting and undercounting rates. Scrutinizing the segmentation results using our spatial-color SC approach, we observed that some undercounted cells were missed because of their significantly lower contrasts compared to surrounding cells. There were only two to seven cells overcounted, and verification revealed they were cells broken into more than one segment, as illustrated in Fig. 1(f).

B. Fetal RBC Counting and Blind KB Tests

To quantify the accuracy of fetal cell identification using supervised learning, 12 slides (three per group) with known fetal cell concentrations (0.1%, 0.25%, 0.5%, and 1%) were tested, in accordance with a research protocol approved by the Mount Sinai Hospital Review Board. These "artificial" KB slides were prepared through accurately controlled mixing of fetal blood

TABLE II
TOTAL CELL COUNTING (UC: UNDERCOUNTED; OC: OVERCOUNTED)

	technologist	marker-controlled watershed			proposed algorithm		
Image	#total	#UC/ratio	#OC/ratio	#total	#UC/ratio	#OC/ratio	#total
1	648	15 / 2.08%	89 / 12.33%	722	7 / 1.09%	4 / 0.62%	645
2	741	12 / 1.44%	105 / 12.59%	834	10 / 1.36%	6 / 0.81%	737
3	607	11 / 1.67%	64 / 9.70%	660	8 / 1.33%	3 / 0.50%	602
4	811	20 / 2.15%	138 / 14.85%	929	12 / 1.49%	5 / 0.62%	804
5	615	16 / 2.38%	72 / 10.73%	671	6 / 0.98%	2 / 0.33%	611
6	762	22 / 2.65%	91 / 10.95%	831	9 / 1.19%	3 / 0.40%	756
7	625	14 / 2.03%	80 / 11.58%	691	7 / 1.12%	3 / 0.48%	621
8	803	16 / 1.76%	123 / 13.52%	910	11 / 1.38%	6 / 0.75%	798
9	505	19 / 3.19%	109 / 18.32%	595	6 / 1.20%	3 / 0.60%	502
10	804	21 / 2.23%	157 / 16.70%	940	9 / 1.12%	7 / 0.87%	802
11	678	15 / 1.92%	120 / 15.33%	783	11 / 1.63%	5 / 0.74%	672
12	651	16 / 2.13%	115 / 15.33%	750	9 / 1.39%	5 / 0.77%	647

TABLE III
COUNTING RESULTS: AUTOMATED COUNTING; MANUAL COUNTING BY TECHNOLOGIST

		automated				
group	slide	#Fetal	#Total	Ratio	technologist	known
1	1	89	74325	0.12%	0.16%	0.1%
	2	62	68941	0.09%	0.19%	
	3	78	70578	0.11%	0.07%	
2	1	179	81454	0.22%	0.20%	0.25%
	2	210	87489	0.24%	0.18%	
	3	230	82045	0.28%	0.31%	
3	1	399	76808	0.52%	0.41%	0.5%
	2	386	80483	0.48%	0.38%	
	3	379	84156	0.45%	0.44%	
4	1	746	73105	1.02%	1.11%	1.0%
	2	787	79514	0.99%	1.20%	
	3	755	77824	0.97%	1.08%	

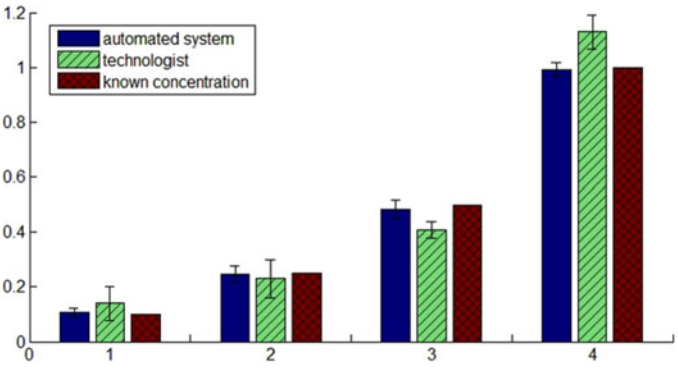

Fig. 8. Comparison between technologist reading and automated counting.

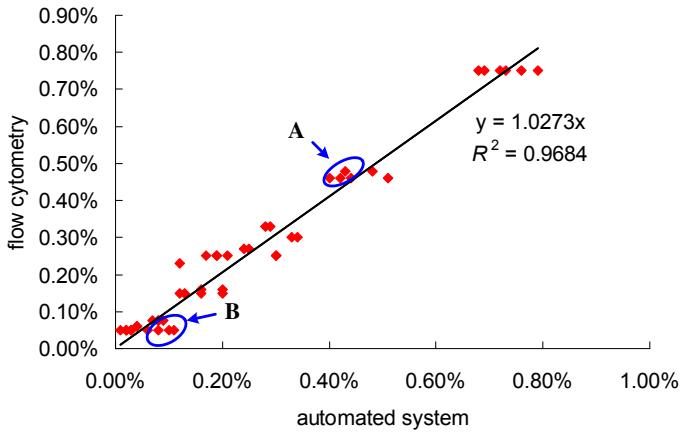

Fig. 9. Correlation between automated counting and flow cytometry in 51 pregnant patient samples ($R^2 = 0.9684$).

from umbilical cord and adult RBCs. Results from automated counting and hospital technologist reading are summarized in Table III.

Data in Table III are graphically shown in Fig. 8. Our automated system determined on the 12 "artificial" KB slides average fetal RBC concentrations to be 0.107%, 0.247%, 0.483%, and 0.993% with standard deviations of 0.015%, 0.031%, 0.035%, and 0.025%. The results from technologist reading were 0.14%, 0.23%, 0.41%, and 1.13% with standard deviations of 0.06%, 0.07%, 0.03%, and 0.06%, respectively. Compared to the known mixing ratios on these "artificial" KB slides, these results quantitatively confirmed the automated system's capability for highly accurate RBC counting. Note that our automated system counted over 60 000 cells per KB slide while standard technologist reading was limited to ~2000 cells. Additionally, automated counting can be completed within 5 min per slide, while manual reading costs more than 15 min.

Another 51 KB slides were made from pregnant patient samples collected in the Mount Sinai Hospital were tested. Testing results using our automated system strongly correlated with those from benchmarking flow cytometry measurement ($R^2 = 0.9684$ shown in Fig. 9 versus $R^2 = 0.9147$ between technologist reading and flow cytometry, data not shown). Counting accuracy is defined as

$$\text{Accuracy} = \frac{\text{TP} + \text{TN}}{\text{TP} + \text{TN} + \text{FP} + \text{FN}} \tag{4}$$

where TP is the number of true positives, FP is the number of false positives, TN is the number of true negatives, and FN is the number of false negatives. The counting accuracy of our

automated system was quantified to be 0.972 ± 0.09 (versus 0.911 ± 0.14 in technologist reading).

C. Discussion

The data points labeled "A" in Fig. 9 are those fetal concentrations determined by the automated system to be lower than flow cytometry. We reevaluated those slides and observed that colors of some fetal RBCs appeared much lighter compared to "canonical" fetal RBCs shown in Fig. 1(a). These lighter fetal RBCs were considered by the automated system negative. For those slides (labeled "B") with higher fetal RBC concentrations than determined by flow cytometry, some negative RBCs appeared darker and brighter than surrounding cells, leading to higher false positives.

HbF+ RBCs (termed *F* cells) can also exist in adults. The number of *F* cells becomes higher in inherited hemoglobin disorders, such as β-thalassaemias, sickle cell anemia, and hereditary persistence of fetal hemoglobin [23]. During pregnancy, maternal hematopoiesis also generates low levels of *F* cells, and low concentrations. In healthy adults, approximately 3–7% of RBCs are *F* cells, containing 20–25% of HbF [24]. After acid elution, *F* cells appear lighter compared to "canonical" fetal RBCs but brighter than maternal cells. It can be challenging in KB test to differentiate fetal RBCs from *F* cells having high amounts of HbF. As our work progresses to involve a larger patient size, the feasibility of properly gating *F* cells will be investigated.

VI. Conclusion

This paper has described an automated system for fetal and maternal RBC reading in a clinical KB test. The system uses a custom-motorized image capturing platform to automatically center a KB slide, collect 120 images (over 60 000 cells), and count/distinguish fetal and maternal RBCs. Spatial-color classification with SC is proposed to effectively count overlapping cells. Multiple features including cell color, size, shape, and contrast variations are used in supervised learning for distinguishing fetal RBCs and maternal ones. Testing patient KB slides, the automated system quantitatively demonstrated high accuracy in counting and strong correlation with benchmarking flow cytometry. Compared to manual technologist reading, the automated system is significantly more efficient and accurate.

Acknowledgment

The authors would like to thank the Department of Pathology and Laboratory Medicine, Mount Sinai Hospital, Toronto, ON, Canada, for patient KB slides preparation.

References

[1] J. M. Bowman, B. Chown, M. Lewis, and J. M. Pollock, "Rh isoimmunization during pregnancy: Antenatal prophylaxis," *Can. Med. Assoc. J.*, vol. 118, no. 6, pp. 623–627, Mar. 1978.

[2] B. H. Davis, S. Olsen, N. C. Bigelow, and J. C. Chen, "Detection of fetal red cells in fetomaternal hemorrhage using a fetal hemoglobin monoclonal antibody by flow cytometry," *Transfusion*, vol. 38, no. 8, pp. 749–56, Aug. 1998.

[3] J. Bowman and J. Pollock, "Rh-immunization during pregnancy and the grandmother theory," *J. Pediatr.*, vol. 93, no. 2, pp. 313–314, Aug. 1978.

[4] C. Chen, S. Cheng, C. Lee, F. Chang, C. Wu, and Y. Yuh, "Fetomaternal Hemorrhage," *J. Med. Sci.*, vol. 23, no. 4, pp. 231–234, 2003.

[5] Z. Wang, J. Shi, Y. Zhou, and C. Ruan, "Detection of red blood cell-bound immunoglobulin G by flow cytometry and its application in the diagnosis of autoimmune hemolytic anemia," *Int. J. Hematol.*, vol. 73, no. 2, pp. 188–193, Feb. 2001.

[6] N. Bandekar, A. Wong, D. Clausi, and M. Gorbet, "A novel approach to automated cell counting for studying human corneal epithelial cells," in *Proc. Int. Conf. IEEE Eng. Med. Biol. Sci.*, Boston, MA, USA, Jan. 2011, pp. 5997–6000.

[7] W. C. Warger, II, J. A. Newmark, B. Zhao, C. M. Warner, and C. A. DiMarzio, "Accurate cell counts in live mouse embryos using optical quadrature and differential interference contrast microscopy," *Proc. SPIE*, vol. 6090, pp. 609009-1–609009-12, Feb. 2006.

[8] D. M. Pelikan, S. A. Scherjon, W. E. Mesker, G. M. de Groot-Swings, G. G. Brouwer-Mandema, H. J. Tanke, and H. H. Kanhai, "Quantification of fetomaternal hemorrhage: A comparative study of the manual and automated microscopic Kleihauer-Betke tests and flow cytometry in clinical samples," *Amer. J. Obstetrics Gynecol.*, vol. 191, no. 2, pp. 551–557, Aug. 2004.

[9] D. Huh, W. Gu, Y. Kamotani, J. B. Grotberg, and S. Takayama, "Microfluidics for flow cytometric analysis of cells and particles," *Physiol. Meas.*, vol. 26, no. 3, pp. R73–R98, Jun. 2005.

[10] Y. Mundee, N. C. Bigelow, B. H. Davis, and J. B. Porter, "Simplified flow cytometric method for fetal hemoglobin containing red blood cells," *Cytometry*, vol. 42, no. 6, pp. 389–393, Dec. 2000.

[11] L. Wong, B. C. Hunsberger, C. Bruce Bagwell, and B. H. Davis, "Automated quantitation of fetomaternal hemorrhage by flow cytometry for HbF-containing fetal red blood cells using probability state modeling," *Int. J. Lab. Hematol.*, vol. 35, no. 5, pp. 548–554, Oct. 2013.

[12] D. M. V. Pelikan, W. E. Mesker, S. A. Scherjon, H. H. H. Kanhai, and H. J. Tanke, "Improvement of the Kleihauer-Betke test by automated detection of fetal erythrocytes in maternal blood," *Cytom. Part B, Clin. Cytom.*, vol. 54, no. 1, pp. 1–9, Jul. 2003.

[13] R. Rodríguez, T. E. Alarcón, and O. Pacheco, "A new strategy to obtain robust markers for blood vessels segmentation by using the watersheds method," *Comput. Biol. Med.*, vol. 35, no. 8, pp. 665–686, Oct. 2005.

[14] D. Gloria, F. Gonzalez, and E. Romero, "Automatic clump splitting for cell quantification in microscopical images," *Prog. Pattern Recognit., Image Anal. Appl.*, vol. 4756, pp. 763–772, 2007.

[15] C. Chen, W. Wang, J. A. Ozolek, and G. K. Rohde, "A flexible and robust approach for segmenting cell nuclei from 2D microscopy images using supervised learning and template matching," *Cytometry A*, vol. 83, no. 5, pp. 495–507, May 2013.

[16] C. Jung and C. Kim, "Segmenting clustered nuclei using H-minima transform-based marker extraction and contour parameterization," *IEEE Trans. Biomed. Eng.*, vol. 57, no. 10, pp. 2600–2604, Oct. 2010.

[17] M. Datar, D. Padfield, and H. Cline, "Color and texture based segmentation of molecular pathology images using HSOMS," in *Proc. IEEE Int. Symp. Biomed. Imag. Nano Macro*, May 2008, pp.292–295.

[18] Y. Sun, S. Duthaler, and B. Nelson, "Autofocusing in computer microscopy: Selecting the optimal focus algorithm," *Microsc. Res. Techn.*, vol. 65, no. 3, pp. 139–149, Oct. 2004.

[19] M. Farhan, O. Yli-Harja, and A. Niemistö, "An improved clump splitting method for convex objects," in *Proc. 7th Int. Workshop Comput. Syst. Biol.*, 2010, pp. 35–38.

[20] J. Shi and J. Malik, "Normalized cuts and image segmentation," *IEEE Trans. Pattern Anal. Mach. Intell.*, vol. 22, no. 8, pp. 888–905, Aug. 2000.

[21] K. R. Zalik and B. Zalik, "Validity index for clusters of different sizes and densities," *Pattern Recognit. Lett.*, vol. 32, no. 2, pp. 221–234, Jan. 2011.

[22] A. Fitzgibbon, M. Pilu, and R. Fisher, "Direct least square fitting of ellipses," *IEEE Trans. Pattern Anal. Mach. Intell.*, vol. 21, no. 5, pp. 476–480, May 1999.

[23] K. Y. Italia, R. Colah, and D. Mohanty, "Evaluation of F cells in sickle cell disorders by flow cytometry—Comparison with the Kleihauer-Betke's slide method," *Int. J. Lab. Hematol.*, vol. 29, no. 6, pp. 409–414, Dec. 2007.

[24] R. S. Franco, Z. Yasin, M. B. Palascak, P. Ciraolo, C. H. Joiner, and D. L. Rucknagel, "The effect of fetal hemoglobin on the survival characteristics of sickle cells," *Blood*, vol. 108, no. 3, pp. 1073–1076, Aug. 2006.

Authors' photographs and biographies not available at the time of publication.